

Probing Galaxy Assembly Bias in BOSS Galaxies Using Void Probabilities

Kilian Walsh,¹ Jeremy Tinker¹★

¹*Center for Cosmology and Particle Physics, New York University, New York*

Accepted XXX. Received YYY; in original form ZZZ

ABSTRACT

We measure the void probability function (VPF) of galaxies in the Baryon Oscillation Spectroscopic Survey (BOSS). The VPF provides complementary information to standard two-point statistics in that it is sensitive to galaxy bias in the most extreme underdensities in the cosmic web. Thus the VPF is ideal for testing whether halo occupation of galaxies depends on large-scale density, an effect known as galaxy assembly bias. We find that standard HOD model—one parameterized by halo mass only—fit only to the two-point function, accurately predicts the VPF. Additionally, for HOD models where density dependence is explicitly incorporated, the best-fit models fit to the combination of the correlation function and the VPF have zero density dependence. Thus galaxy assembly bias is not a strong source of systematic uncertainty when modeling the clustering of massive galaxies.

Key words: cosmology: observations – galaxies: statistics – galaxies: haloes

1 INTRODUCTION

The growth of structure in the dark matter content of the universe leads to the formation of regions of high relative density over time and, contrastingly, also regions of significant sparsity in the matter field. Galaxies act as a biased tracer of the underlying dark matter density field (see Desjacques et al. 2018 for a thorough review of large scale galaxy bias), so these regions of sparsity lead to the existence of large voids within the galaxy distribution (see the review of van de Weygaert & Platen 2011). Since the discovery of voids that were larger in extent than typical galaxy clusters (Gregory & Thompson 1978), they have been considered a probe of interest for the study of cosmology and large scale structure formation (see e.g. Betancort-Rijo et al. 2009, Einasto et al. 2011, Lavaux & Wandelt 2012, Clampitt et al. 2016, Kitaura et al. 2016, and Mao et al. 2017 for recent examples).

Voids also present a useful probe to understand the nature of galaxy formation. It is known that galaxies found in voids are typically spiral/irregularly-shaped and found to be HI rich, having low luminosity and stellar mass, and small size relative to the general population of galaxies (Tavasoli et al. 2015, Beygu et al. 2017, and Pustilnik et al. 2019). This suggests that galaxy formation and evolution may have a dependence on the large scale dark matter density. Controlling for factors such as galaxy mass, or the halo abundances

found in underdense regions of simulations, there are also studies done in the context of voids which claim to find no special relationship between galaxies and their environment (Patiri et al. 2006; Croton & Farrar 2008; Tinker et al. 2008a; Tinker & Conroy 2009).

It is well established, theoretically and in high-resolution dark matter simulations, that the properties of dark matter halos in Λ CDM cosmologies – such as halo mass (Press & Schechter 1974; Mo & White 1996) and formation time (Sheth & Tormen 2004; Wechsler et al. 2006; Zentner 2007; Dalal et al. 2008) – are also strongly dependent on their large-scale dark matter overdensity. As such, the observed correlations of galaxy properties with environment may be explained with a model that connects galaxies with halos.

One of the chief models of the galaxy-halo connection is the Halo Occupation Distribution (HOD; see the review of the galaxy-connection by Wechsler & Tinker (2018)). The HOD parameterizes the bias between galaxies and dark matter by the statistical relationship between dark matter halos and the number of galaxies within them (e.g., Scoccimarro et al. 2001; Berlind & Weinberg 2002; Cooray & Sheth 2002). The HOD has been remarkably successful in explaining a host of observational phenomena (e.g., Zehavi et al. 2011, Tinker et al. 2012, Reid et al. 2014, and Coupon et al. 2015). In its most basic form, the HOD parameterizes the occupation of a halo by galaxies based only on the mass of the halo. However, recent studies have suggested that there may be “assembly bias” in galaxy occupation, whereby the

★ e-mail: jeremy.tinker@nyu.edu

occupation of dark matter halos may depend on properties other than mass (Reddick et al. 2013; Zentner et al. 2016; Lehmann et al. 2017). Physically, this would manifest as a correlation between galaxy formation efficiency and that large-scale environment of a galaxy at fixed halo mass. Tinker et al. (2006) proposed using void statistics, in combination with two-point statistics, to determine if such a correlation exists. The two-point correlation function is sensitive to halos in mean and high-density environments, where most pairs are found, while voids are defined by halos in the most extreme low-density regions of the universe. If galaxy formation efficiency changes from high to low densities, one could not simultaneously fit both statistics using an HOD model that parameterizes occupation solely on halo mass. Zentner et al. (2014) found similar results using abundance matching models of galaxy bias to construct color-defined galaxy samples. Using this technique, Tinker et al. (2008b) found that the galaxies in the Sloan Digital Sky Survey (York et al. 2000) could be fit with this mass-only approach. Any correlation of the HOD with large-scale environment could only be minimal, or else the models could no longer fit both statistics.

In this work, we extend the investigation of the HOD for a far larger sample of galaxies, at higher redshifts, by performing this test using data from the Baryon Oscillation Spectroscopic Survey (BOSS; Dawson et al. 2013). Unlike the SDSS, the BOSS survey is designed for cosmological inference. Attempts to use BOSS clustering at non-linear scales require a full model for galaxy bias at those scales (Reid et al. 2014; Rodríguez-Torres et al. 2016; Zhai et al. 2018). If galaxy assembly bias exists and is not included in the bias model, the cosmological constraints will themselves be biased (McCarthy et al. 2018). The BOSS galaxy sample also differs from the low-redshift SDSS samples in that the target selection includes complicated cuts in galaxy color-space, and does not yield a strict volume-limited sample (Reid et al. 2016). To perform this test, we make comparisons with mock measurements made in simulated galaxy populations derived using the HOD with the high resolution simulation from the MultiDark collaboration (Riebe et al. 2013a), MDPL.

The remaining sections of the chapter are organized as follows: Section 2 describes the BOSS data in detail and the procedure of making measurements of the 2-point correlation function and void probability function; Section 3 describes the HOD model for galaxy occupation of halos, with and without environment dependence, and how the mock measurements of the correlation function and VPF are made; Section 4 presents our findings for the HOD model when applied to the BOSS data; and in the final section, we offer our concluding remarks.

2 DATA & MEASUREMENTS

2.1 BOSS Data

BOSS (?) is one of the spectroscopic surveys of SDSS-III (Eisenstein et al. 2011), comprising 1.5 million galaxies and intended to measure the Baryon Acoustic Oscillation (BAO) feature (see Weinberg et al. 2013 for a review). The full survey spans 10,000 square degrees and probes up to redshift

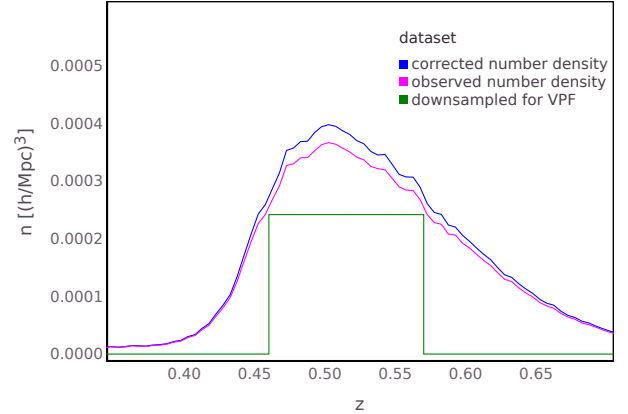


Figure 1. This figure shows the number densities as a function of redshift for the observed CMASS NGC galaxy sample, the corrected number density when accounting for fibre collisions, and the sample used for the VPF measurement that has a constant number density within the redshift range $z = [0.4575, 0.5725]$.

$z = 0.8$. Target selection for the CMASS sample used here is described in Reid et al. (2016). All results here use Data Release 11 of the SDSS, the penultimate data release of BOSS, which comprises roughly 85% of the full footprint. Additionally, we restrict our analyses to the North Galactic Cap region (NGC), which is the bulk of the BOSS footprint, yielding a total sample covering roughly 6,000 deg².

2.2 Data Preparation

Our probe of void statistics is the void probability function (VPF) which we will define presently. The VPF is highly sensitive to sample number density, thus we restrict the BOSS data to a range of redshift for which the number density is above some threshold. We then randomly subsampled the data within this redshift interval such that the remaining galaxies would have a constant number density at comoving volume in redshift bins in that range. The redshift range we chose for the Northern Galactic Cap (NGC) CMASS (the high-redshift portion of BOSS targets) galaxies was $z = [0.4575, 0.5725]$ such that the number densities of the remaining galaxies was 65% of the peak number density of the sample. These values were chosen as a compromise between maintaining a high number density while also probing a large volume of the sample by not overly restricting the redshift range. The resulting galaxy sample has just under 500,000 galaxies. We randomly subsample the galaxies at each location in redshift, rather than a more complicated selection, due to that fact that the clustering of CMASS galaxies is roughly constant with redshift (White et al. (2011)). Figure 1 shows the number density of the downsampled galaxies as a function of redshift, compared with the original sample and with the corrected number density, which is discussed in the following section.

2.3 Correlation Function Measurements

To quantify two-point clustering we use the projected correlation function $w_p(r_p)$ (Davis & Peebles 1983). This function is defined as the integral of the two-dimensional clustering measurement $\xi(r_p, \pi)$ along the line-of-sight direction π and is insensitive to redshift space distortions, while offering good constraints on HOD parameters through its signals on small projected scales r_p :

$$w_p(r_p) = 2 \int_0^{\pi_{\max}} \xi(r_p, \pi) d\pi, \quad (1)$$

with $\pi_{\max} = 80 \ h^{-1}\text{Mpc}$. We use the Landy-Szalay estimator (Landy & Szalay 1993) for two-point statistics. We also choose 24 logarithmic spaced bins in r_p in the range $[0.3, 60.0] \ h^{-1}\text{Mpc}$.

Due to the size of spectroscopic fibres used to take the galaxy redshift data, and the limited number of overlapping regions in the survey geometry, a significant fraction of target BOSS galaxies were subject to fibre collisions where only one galaxy in a collided pair was observed (more details in e.g. Anderson et al. 2014, Ross et al. 2017). In our measurements, it was necessary to correct for the missing galaxy pairs that lie within the fibre collision angular radius of $62''$, which corresponds to a projected separation of around $r_p \sim 0.4 \ h^{-1}\text{Mpc}$ at the CMASS mean redshift and thus has a big impact on small scale clustering. To estimate the true clustering, we use the method of (White et al. 2011) and upweight the pair counts of any pair found within that separation to account for the missing pairs. The extra weighting factor was determined by finding the ratio of angular clustering measurements $w(\theta)$ between the BOSS galaxies and the photometric SDSS data from the same field. We find we should use a factor of 2.63 to upweight pairs whose galaxies are within $62''$ of one another. The corrected number density of the CMASS galaxies, after accounting for the missing galaxies due to fibre collisions and other systematic factors, is shown in Figure 1.

To make a direct comparison of the galaxies and underlying dark matter distribution with both the w_p and VPF measurements, we restricted the galaxies to the same redshift range as is used for the VPF measurement before counting the pairs. We don't randomly subsample the galaxies as is done for the VPF sample. A random sample of galaxies will still have the same clustering properties as the full original sample and therefore this extra step would only increase uncertainty in the w_p measurement. The results of this measurement are shown in Figure 3, along with the measurements of the VPF, described in the next section.

2.4 VPF Measurements

The void probability function measurement $P_0(r)$ is made by randomly placing spheres of some radius r in many locations of the survey and counting the fraction of empty spheres. Assuming shot noise error in the number of empty spheres found, an appropriate number of spheres must be placed to make a reasonable determination of P_0 . As sphere scale r increases, empty spheres become increasingly rare and more spheres are required to find any signal. Based on the rarity of void spheres above $35 h^{-1}\text{Mpc}$ within our survey volume,

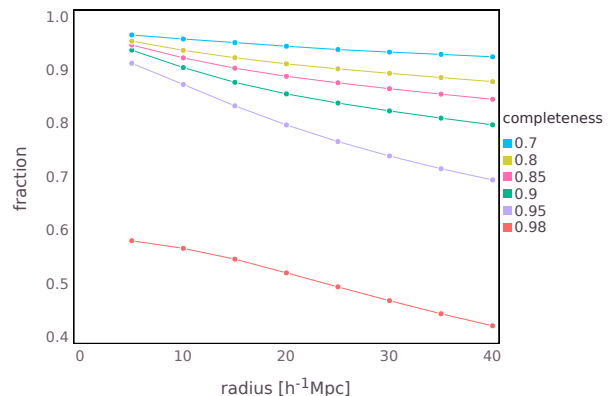


Figure 2. As a test for an appropriate completeness threshold, we test the fraction of spheres which meet a given threshold in the CMASS survey geometry. This plot shows the fraction as a function of sphere radius for a range of thresholds, as described in Section 2.4.

and the computational cost of searching sufficient spheres at that scale, we have made a VPF measurement for voids in the range $[5, 35] \ h^{-1}\text{Mpc}$ in steps of $5 \ h^{-1}\text{Mpc}$, using random samples of up to 10^7 spheres at each radius.

Due to the nature of the survey geometry, which has irregular borders along with missing points in its interior due to stars and other features, not all possible spheres with centres lying within the survey mask will be fully contained within the survey. As such, care must be taken to ensure that a given sphere can be said to truly be a void sphere. Thus, before assessing whether spheres are devoid of galaxies or not, we must first assess whether they are valid survey spheres. In order to be considered as such, we require any sphere that is accounted for in the VPF measurement to meet a completeness threshold, whereby a minimum volume of the sphere is found to be within the survey. We tested the fraction of conserved spheres at each radius for a range of completeness thresholds by randomly proposing spheres within the survey mask and estimating the percentage of the sphere volume that lay outside the mask by using random "veto points" placed at the survey edges and in the interior points that were compromised. The results after averaging the volume over 10^7 spheres at each radius are shown in Figure 2. We decide that spheres up to 95% completeness result in a sufficiently large fraction being conserved for the VPF measurement, where over two thirds of spheres are still valid even up to $40 \ h^{-1}\text{Mpc}$. We will describe our method of making proper comparisons between the mocks and data in the next section.

The results for the CMASS northern sample are shown in Figure 3 along with the w_p measurement for the same galaxies. Errors are described in the following subsection.

2.5 Estimating Covariances with Mock Samples

We determine an estimate of the covariance in our measurements by using a set of mock galaxy samples that were made for the purpose of constructing covariance matrices for the CMASS survey data. The mocks used were the quick par-

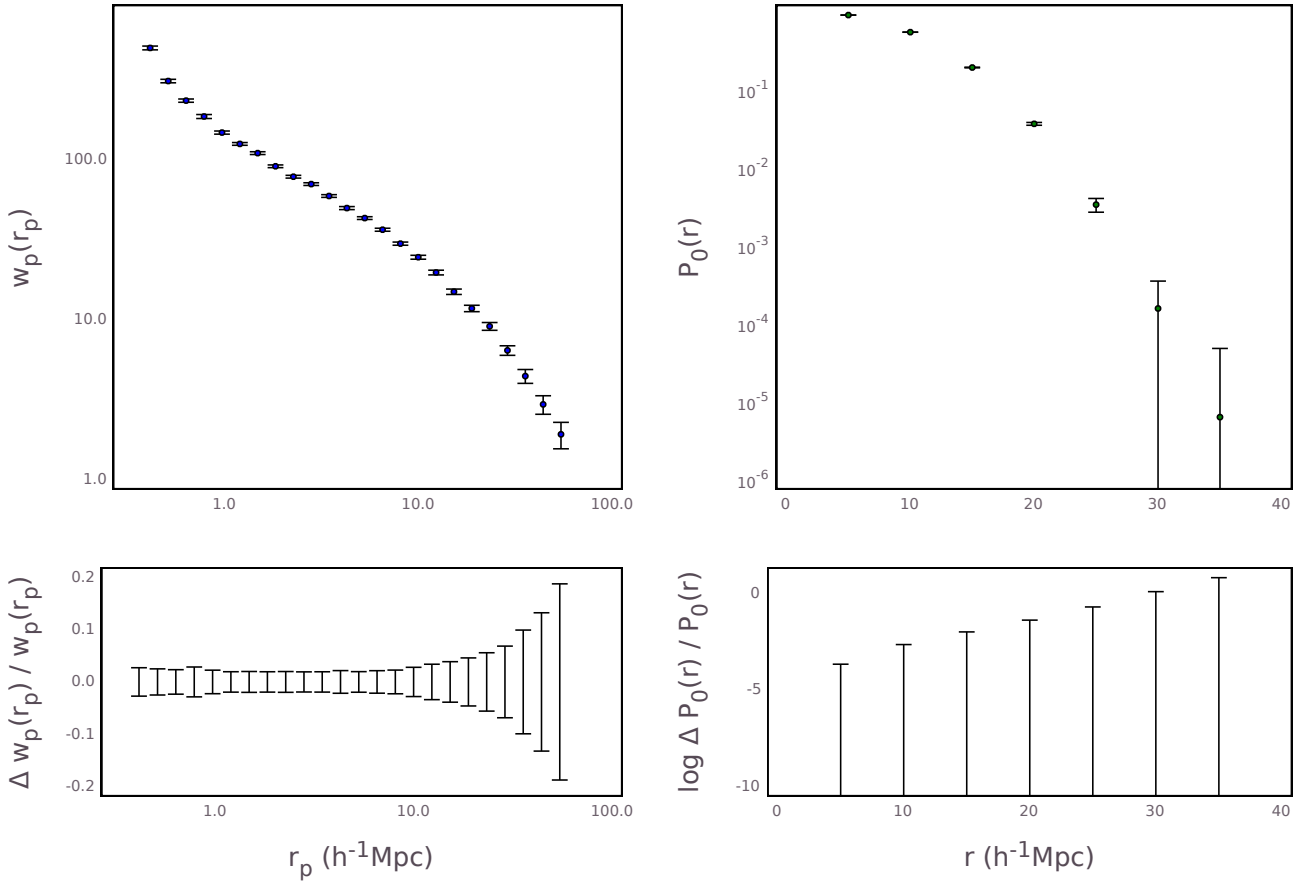


Figure 3. This figure shows the projected correlation function w_p with fractional errors and void probability function with fractional errors. The errors of the VPF are shown in log space since they increase effectively exponentially with void radius.

ticle mesh (QPM) mocks (White et al. 2014) created for BOSS. We made the measurements to match the methods described in the previous sections exactly, using the same estimators and bins and radii, and found the full covariance of these measurements over a set of 400 mocks. The covariance matrix we calculate using these mocks is used for making parameter inference of the HOD model, as described below. The diagonal variances of the matrix were used to determine the errorbars in the measurements shown in Figure 3. For the VPF, we show the fractional error bars in log-space, as the range is very broad. At small scales, the VPF does not contain significant information about large scale structure and the errors are consistent with simple Poisson errors. However, at scales larger than the mean galaxy spacing (roughly $16 h^{-1}\text{Mpc}$) the amplitude of the VPF is reflective of the structure, but the fractional error bar is significantly larger. This is both due to the rarity of empty spheres at these scales and sample variance in the clustering of galaxies.

3 GALAXY CLUSTERING AND VOIDS FROM A HALO OCCUPATION MODEL

3.1 Dark Matter Simulation and Halo Catalogue

To compare the measurements with models of halo occupation, we use a halo catalogue from a high resolution dark matter simulation. For this work we use the Big MultiDark Planck (BigMDPL) simulation (Prada et al. 2012; Riebe et al. 2013b). The simulation has $2.5h^{-1}\text{Gpc}$ comoving volume and 3840^3 dark matter particles, giving it a mass resolution of $2.359 \times 10^{10} h^{-1} M_\odot$. It uses a Planck cosmology (Planck Collaboration et al. 2018) with $h = 0.6777$, $\Omega_\Lambda = 0.693$, $\Omega_M = 0.307$, and $n = 0.96$. The simulation was performed using GADGET-2 code (Springel 2005) and further details can be found in Klypin et al. (2016). The Planck cosmological parameters are used throughout this work to remain consistent with the simulation.

The MultiDark Database also provides halo catalogues for each simulation, which we use for our analysis. The catalogues were made using the Rockstar Halo Finder (Behroozi et al. 2013). We use the host halos from this catalogue – those not contained within the virial radius of any other halo as subhalos – for the purposes of our model. The halos have masses M_{200} determined from their spherical overden-

sity, measured for spheres of $\Delta = 200$ times the critical density. To compute the halo concentration for the halos in the catalogue, we use the empirical relationship found in [Dutton & Macciò \(2014\)](#) for halo masses of this definition at a redshift of $z = 0.5$.

We have also received dark matter particle data from the MultiDark authors with which to measure the dark matter overdensity at $15 h^{-1}\text{Mpc}$ scales at the locations of each of the host halos. We use these halo properties, along with their relative positions and velocities in the simulation, to build model galaxy catalogues with which to estimate galaxy clustering.

3.2 Halo Occupation Distribution

To construct model galaxy catalogues from the halos, we use the Halo Occupation Distribution (HOD) described in [Zheng et al. \(2007\)](#). This is a statistical prescription for the number of central and satellite galaxies that live in a given halo, depending on the mass of that halo. For centrals, there can be either zero or one galaxy, with the mean central occupation at any mass given by

$$\langle N_{\text{cen}} \rangle_M = \frac{1}{2} \left[1 + \text{erf} \left(\frac{\log M - \log M_{\text{min}}}{\sigma_{\log M}} \right) \right], \quad (2)$$

where M_{min} is the halo mass at which the probability for a galaxy existing at its centre goes from less than a half to greater than a half, and $\sigma_{\log M}$ effectively determines the scatter in halo mass between halos with no central galaxies and halos which all have a central galaxy. If a halo has a central galaxy, drawn from a Bernoulli distribution with probability $\langle N_{\text{cen}} \rangle$ the galaxy is given the position and velocity of the halo centre of mass.

The average number of satellite galaxies in a host halo of mass M is given by

$$\langle N_{\text{sat}} \rangle_M = \frac{1}{2} \left[1 + \text{erf} \left(\frac{\log M - \log M_{\text{min}}}{\sigma_{\log M}} \right) \right] \left[\left(\frac{M}{M_1} \right)^\alpha e^{-\frac{M_{\text{cut}}}{M}} \right], \quad (3)$$

which is a slight modification of the original Zheng formulation. It consists of a power law in halo mass, scaled by M_1 with slope α , modulated by the central occupation relationship and with an extra exponential cutoff M_{cut} . The satellite number for each individual halo is drawn from a poisson distribution with mean $\langle N_{\text{sat}} \rangle$ (only if the halo has a central galaxy) and these galaxies are placed around the halo centre according to an NFW profile with the halo's concentration. The satellites are given velocities assuming an isotropic distribution of virialized objects in the halo's gravitational potential.

3.3 Modeling Assembly Bias

To determine whether there is any environment-dependent bias in the galaxy occupation of dark matter halos which is independent of the halo mass, we use the dark matter overdensity of host halos. We measure the relative density ρ of a halo by counting the number of dark matter particles in a sphere of $15 h^{-1}\text{Mpc}$ located at the halo's centre of mass and

dividing by the average number expected over the whole simulation, for a random subsample of dark matter particles for the simulation. [Tinker et al. \(2006\)](#) and [Tinker et al. \(2008b\)](#) used a simple model where halo occupation changed by a set amount at densities below some critical density. The results of [Tinker et al. \(2006\)](#) demonstrated that a model of this kind could produce changes to both $w_p(r_p)$ and the VPF, but that the VPF was far more sensitive to these changes and could be detected to high significance even when the change to $w_p(r_p)$ was negligible within the statistical precision of the measurements.

Here, we extend the method of [Tinker et al. \(2006\)](#) to increase the flexibility of the model. We modify the HOD described above by changing the value of $\log M_{\text{min}}$ as a function of ρ . For each halo, we add an offset to $\log M_{\text{min}}$ of

$$\Delta M_{\text{min}} = \frac{f_\rho}{2} \left[1 + \text{erf} \left(\frac{\log \rho - \log \rho_{\text{th}}}{\sigma_\rho} \right) \right]. \quad (4)$$

This leads to a change in the minimum halo mass for which a halo will be occupied by central galaxies and also changes the modulation of the satellite galaxy occupation by the same factor. The value for M_{min} is effectively changed to have two regimes of halo occupation – one value at higher densities, and another value at lower densities, with a difference in \log of f_ρ that is separated by a threshold density ρ_{th} with a soft transition dictated by σ_ρ . This model allows us to assess whether the data allow for a mechanism of galaxy-formation that prefers galaxies to be formed in halos of the same mass when they occur in different environments.

The choice of parameterization in Equation (4) is meant to give maximum flexibility to the model. It allows galaxy formation efficiency to both increase or decrease in voids, it changes the density scale at which this change can happen, and the rapidity with which the change happens along the edge of the void. Figure 4 shows several examples of how shifts in the mass scale impact clustering. We also compare these results to a model of assembly bias where galaxies are assigned to halos using the abundance matching approach, with galaxy luminosity matched to the peak maximum circular velocity over the history of each halo (see [Wechsler & Tinker 2018](#) for a review of abundance matching methods). Peak circular velocity is also correlated with large scale density at fixed halo mass, thus imprints an assembly bias signal on the galaxy population without explicitly using the large-scale density. However, the change to the clustering created by this abundance matching model is easily within the parameter space of equation (4). But we don't wish to restrict ourselves to only the types of assembly bias created in this way—thus, the increased flexibility of equation (4) is more appropriate for the purposes of this study.

3.4 Modeling Galaxy Clustering

3.4.1 Projected Correlation Function

Using the halo catalogue and HOD described above, we can simulate a galaxy catalogue which we can use to make model measurements to compare with the measurements made in the data. As described in Section 2.3, the projected correlation function measurement made in the CMASS sample has been corrected for any geometric effects and fibre collisions through the use of a carefully constructed random

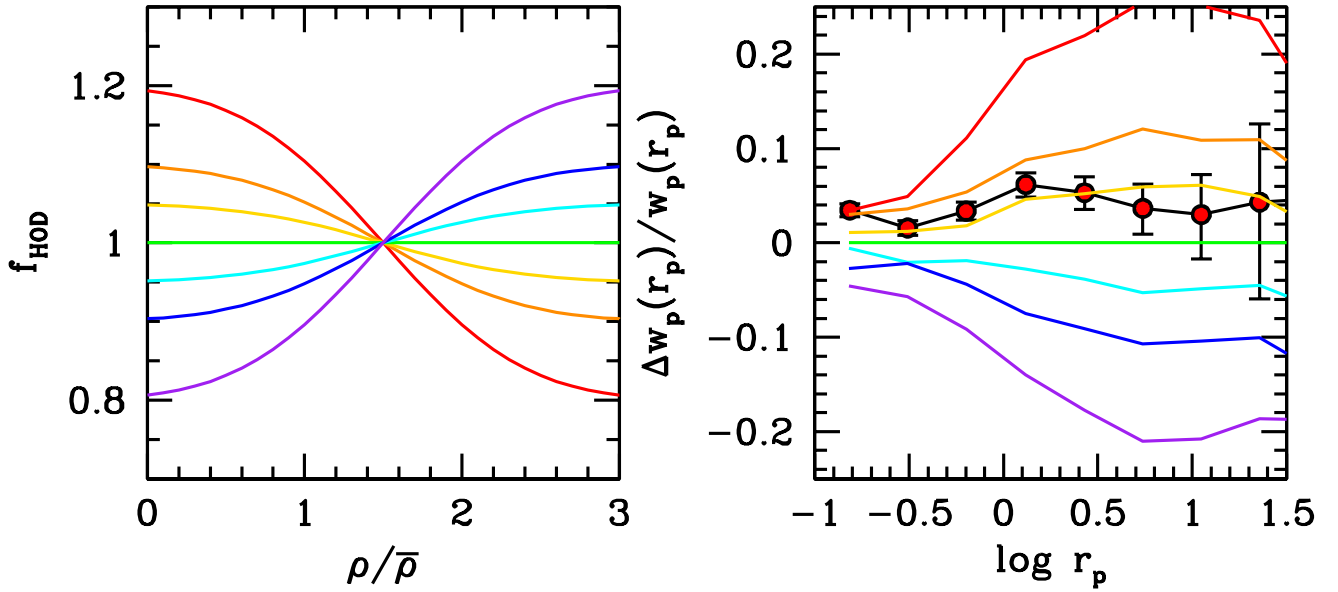


Figure 4. Our model for incorporating galaxy assembly bias. The left-hand panel shows several implementations of equation (4). Here f_{HOD} is the fractional change to the HOD mass scale. The parameters σ_p and ρ_{th} are held constant, but f_p is varied to both increase and decrease galaxy formation efficiency at densities below the mean density around CMASS galaxies. The right-hand panel shows the impact these variations have on the two-point clustering of galaxies. The points with errorbars show the amount of assembly bias predicted in a model where galaxy mass is matched to peak circular velocity of the halo, which is correlated with halo formation history. The points themselves show the clustering of this model relative to a shuffled version of the same model, where galaxies are shuffled randomly between halos of the same mass, thereby erasing any correlations with the large-scale density field, but preserving the HOD. The expected assembly bias is small, and can be easily modeled in our framework.

point distribution over the survey mask and with collision pair-upweighting. Therefore, we need not make any special considerations in our model measurement. We make a distant observer approximation for the simulation box and take one dimension to be the line-of-sight axis. Along this dimension x_3 , we displace each galaxy according to its parallel velocity v_3 by

$$\Delta x_3 = \frac{1+z}{H(z)} v_3 \quad (5)$$

to mimic redshift-space distortions, where $H(z)$ is the Hubble parameter at the simulation redshift z .

We use the updated galaxy positions to calculate the pairs for the $\xi(r_p, \pi)$ estimator with π along the x_3 dimension of the box. Since the box is periodic, we can analytically compute the expected random pairs for the estimator by assuming a poisson process to save on computational time. The code we use for calculating the theory $w_p(r_p)$ is `Corrfunc` (Sinha & Garrison 2017).

3.4.2 Void Probability Function

In order to make an honest comparison of the simulated galaxies to the observed galaxies with respect to the VPF, we must first match the galaxy number density. We downsample the simulated galaxies randomly until we reach the same constant number density as we had for the redshift range for

the VPF measurement discussed in Section 2.2 and shown in Figure 1.

Since the measurement of the VPF made in the data was made using a sample of galaxies with missing observations due to fibre collisions, it was necessary to also simulate such fibre collisions in our mock galaxies. Otherwise, down-sampling the simulated galaxy sample to our chosen number density would lead to more voids, since there would be no preferential removal of collided pairs, which are typically in denser regions. Removing “fibre collisions” first in our simulated mock leads to a smaller fraction of voids at increasingly larger radii.

The comoving distance from the nearest galaxies to the furthest in our observed sample is approximately $300 h^{-1}\text{Mpc}$. The depth of the simulation box, along our line of sight dimension, is far greater, at $2500 h^{-1}\text{Mpc}$. The number of galaxy pairs that will seem to be “collided” by the fibre collision radius of our simulation redshift (which comes to $\sim 0.4 h^{-1}\text{Mpc}$ in comoving separation) is thus also far greater in the box than in the survey. It becomes an issue to obtain the desired number density in our mock because there can be enough collided galaxies, that removing the same fraction of them as are unobserved in the data, leads to a lower mock number density than the final data sample. As a workaround, we restrict the simulation to a fraction of its size along the line-of-sight dimension. To be as consistent with the survey data as possible, we choose the fraction such that the ratio of simulation box “depth” to “area”, is similar to the ratio of

survey depth and area. The full survey volume is approximately $10^9 h^{-3} \text{Mpc}^3$, so we choose our effective depth for the simulation box to be $600 h^{-1} \text{Mpc}$ and make the measurement in this restricted portion of the mock volume.

Once we have removed collided mock galaxies appropriately and sampled the mock down to match the observed constant number density sample, we measure the VPF in the mock. We make the measurement with 10^7 spheres at the largest radii, as in the data, and use random points distributed evenly throughout the mock. The mock is assumed periodic in the transverse dimensions, but voids are kept one sphere radius from the edges in the restricted line-of-sight dimension.

3.5 Fitting HOD Parameters to the Measurements

To fit the model values for w_p and $P_0(r)$ to the observed values, we use a standard χ^2 statistic. We compute the statistic for samples in the HOD parameter space of M_{\min} , $\sigma_{\log M}$, M_1 , M_{cut} , and α (and including f_ρ , ρ_{th} , and σ_ρ for the density dependent model). For each sample, we populate the halo catalogue with galaxies accordingly and then compute the simulated measurements. The samples are drawn from a posterior distribution obtained by multiplying the χ^2 values with prior probabilities, chosen to have flat distributions within physically reasonable ranges.

Any implementation of an HOD requires the number density of the sample to be modeled. For the CMASS sample, which has a variable number density, the choice of which density to use is not entirely clear. Here we use the mean corrected number density within the redshift range of our sample. The sample variance on this value is very small, at the percent level, but we allow the number density of the HOD model to vary by $\pm 10\%$ relative to the mean. This incorporates the possibility that the mean value is not the most appropriate, and marginalizes over other possibilities. For each mock, however, the VPF is always measured after downsampling the mock to the same value as the CMASS sample on which we make our VPF measurements. The posteriors are sampled using a Markov Chain Monte Carlo (MCMC) sampler based on an affine-invariant search algorithm (Goodman & Weare 2010).

We perform the fit for multiple configurations of the model and measurements. In the first experiment, we fit only to the w_p measurement, using the standard, non-density dependent HOD, to get a fiducial set of posteriors and compare the VPF distribution of the mocks from the posterior samples to the observed VPF. We make another fit with the standard HOD, fitting to both w_p and the VPF P_0 . Finally we make a fit using the density-dependent HOD, fitting to both the w_p and P_0 .

4 RESULTS

The comparison of posterior predictions for both w_p and P_0 for the fiducial fit (constrained using only w_p) are shown in Figure 5. The fiducial model provides a good fit to the VPF, despite only using the information of the two-point function in the data to constrain the model. This suggests already

that there is no need for the inclusion of density dependence in the galaxy-halo model to describe galaxy clustering statistics that are sensitive to a range of densities within the cosmic web.

As a confirmation of this lack of density dependence in halo occupation, we show the posterior parameter distributions of a model including density dependence – as described in Section 3 – in Figure 6. The density parameters, particularly the offset magnitude f_ρ are all consistent with having no impact on the model. An analogous comparison of the predictions for w_p and P_0 as in Figure 5, but made using the HOD including this density dependence, is shown in Figure 7. Unsurprisingly, there is similarly good correspondence with the data.

A table summarizing the maximum a posteriori values along with the standard deviation of marginalized samples in each parameter, for each of the model cases, is shown in Table 1. This includes the test where we simultaneously fit both the w_p and P_0 for the density-independent model. As expected from Figure 5, the parameter constraints are consistent with the model in which only w_p is fit. The only significant difference is in M_{cut} , but the difference is only in the numerical values—at such small values of M_{cut} , the cutoff in the satellite occupation function has no quantitative impact on the clustering because it is so much smaller than M_{\min} . The agreement on the HOD parameters extends to the density-dependent model as well. The best-fit value of f_ρ is 0.02 ± 0.04 , clearly consistent with zero—i.e., no density dependence. Indeed, values significantly away from zero are strongly excluded by the data.

5 DISCUSSION

We have shown that the information on galaxy bias encoded in the galaxy two-point correlation function is sufficient to model galaxy bias in extremely low-density environments. Thus, halo occupation does not change from high to low densities. Additionally, incorporating a flexible model for galaxy assembly bias—a model in which halo occupation depends on both M_h and large-scale density—only fits the combined w_p and VPF data when the density-dependent parameters are consistent with zero. Studies meant to extract cosmological information from non-linear clustering of large-scale galaxies redshift surveys, like BOSS, it’s successor eBOSS (Dawson et al. (2015)) and the near-term DESI survey (DESI Collaboration et al. (2016)), can expect minimal-to-no degeneracies between cosmology and assembly bias.

This result appears to be in tension with those of Saito et al. (2016), where measurements of w_p are better fit using an age-matching model for galaxy occupation in a halo-abundance matching context. However, the results of Saito et al. (2016) are mostly inferred from redshift-dependent effects in their model, which we do not encounter, given the relatively narrow redshift range of this work. Another difference is our implementations of assembly bias, which in our model is done explicitly through a dependence on ρ , and in theirs done implicitly through abundance matching. However, Figure 4 shows that the type of assembly bias imparted in this model is within our parameter space. Additionally, Goh et al. (2019) find that the properties of dark matter halos, once controlling for large-scale density, are indepen-

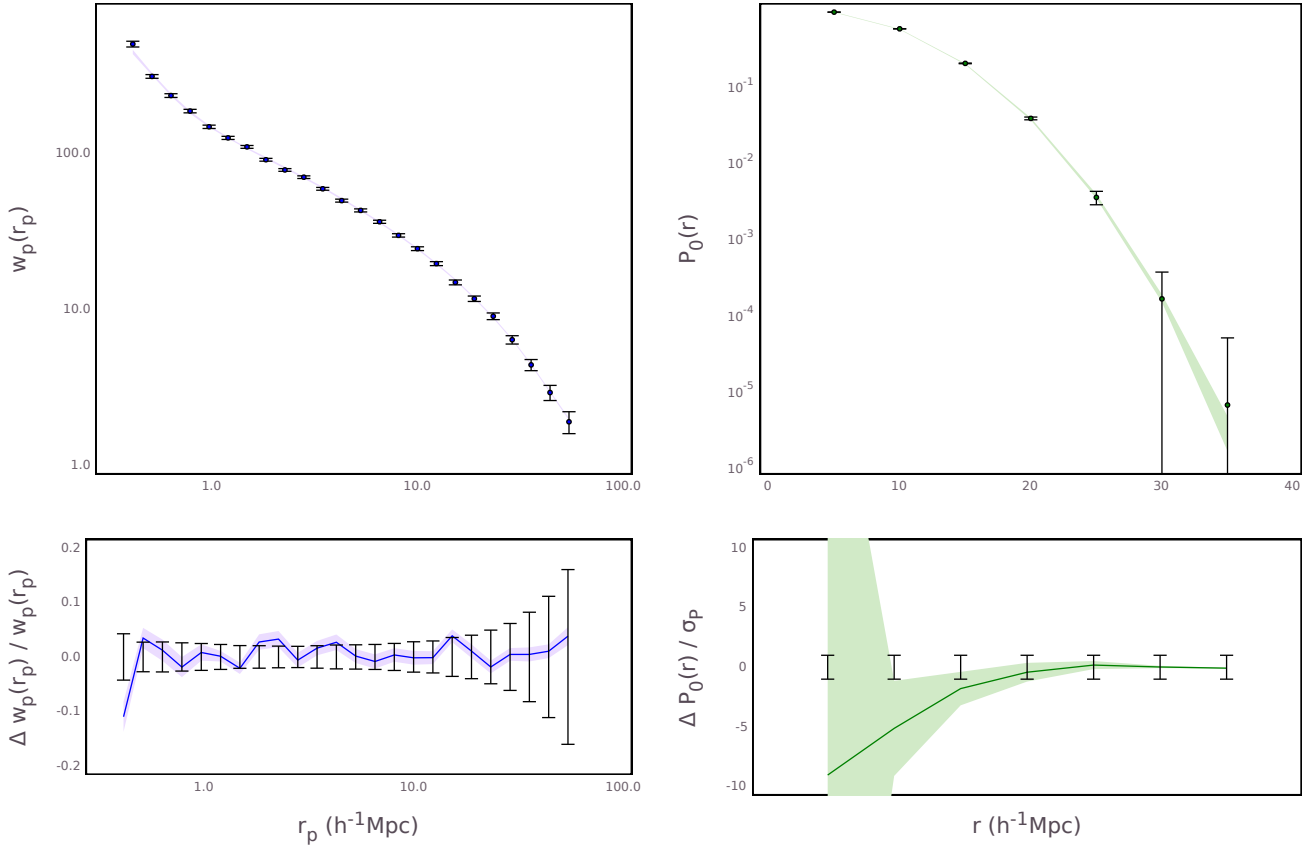


Figure 5. This figure shows the same measurements as in Figure 3 and includes the predicted values from mock measurements in simulated galaxy samples. The mock galaxies are derived from parameter samples from the posterior over the HOD parameters, obtained from fitting the standard HOD using the w_p measurement. The model predictions show a region within one standard deviation of the predictions from the posterior. In the residual plot for the VPF (lower right panel) we compare model predictions as a distance in standard deviations (i.e. the observation errors) in order to clearly show the values in each bin.

Table 1. This table shows the top hat prior ranges (in some cases improper) along with the maximum a posteriori values and standard deviations from the posterior chains of our models. The three sets of posteriors are taken from a model fit only to the two-point function, a model with mass-only HOD fit to both the two-point function and VPF, and a model fit to both and incorporating density dependence in the HOD. The constraints are consistent across all models, showing that a mass-only model is sufficient to fit the data and that assembly bias in the BOSS LRGs is strongly ruled out.

parameter	priors	w_p only	w_p & P_0	w_p & P_0 with f_ρ
α	[0,3]	1.17(06)	1.12(16)	1.00(23)
M_{cut}	$(-\infty, \infty)$	-17.47(1150)	4.87(17)	8.00(29)
M_1	$[M_{\text{min}}, 15]$	14.2(03)	14.28(17)	14.22(17)
M_{min}	[10.5, 15]	13.07(04)	13.18(13)	12.92(14)
$\sigma_{\log M}$	(0, 1.5]	0.35(06)	0.55(13)	0.45(25)
f_ρ	$[10.5 - M_{\text{min}}, 15 - M_{\text{min}}]$			0.02(04)
ρ_{th}	[0.5, 1.5]			1.02(11)
σ_ρ	(0, ∞)			0.03(01)

dent of the details of the halo’s location within the cosmic web—i.e., filaments, walls, nodes, sheets, etc. Thus there is not more information beyond ρ required when implementing assembly bias.

The ability of the density-independent HOD model to match both the clustering and void distribution is somewhat surprising given recent results showing that a mass-only approach has difficulty yielding statistically acceptable fits to

the galaxy correlation function for low-luminosity samples in SDSS (Reddick et al. 2013; Zentner et al. 2016; Lehmann et al. 2017). All of these works found a better fit when correlating halo occupation with something other than mass, either through an explicit second parameter (i.e., the ‘decorated HODs’ of Hearin et al. 2016), or by abundance matching on galaxy properties other than mass. However, both Zentner et al. (2016) and Lehmann et al. (2017) show no

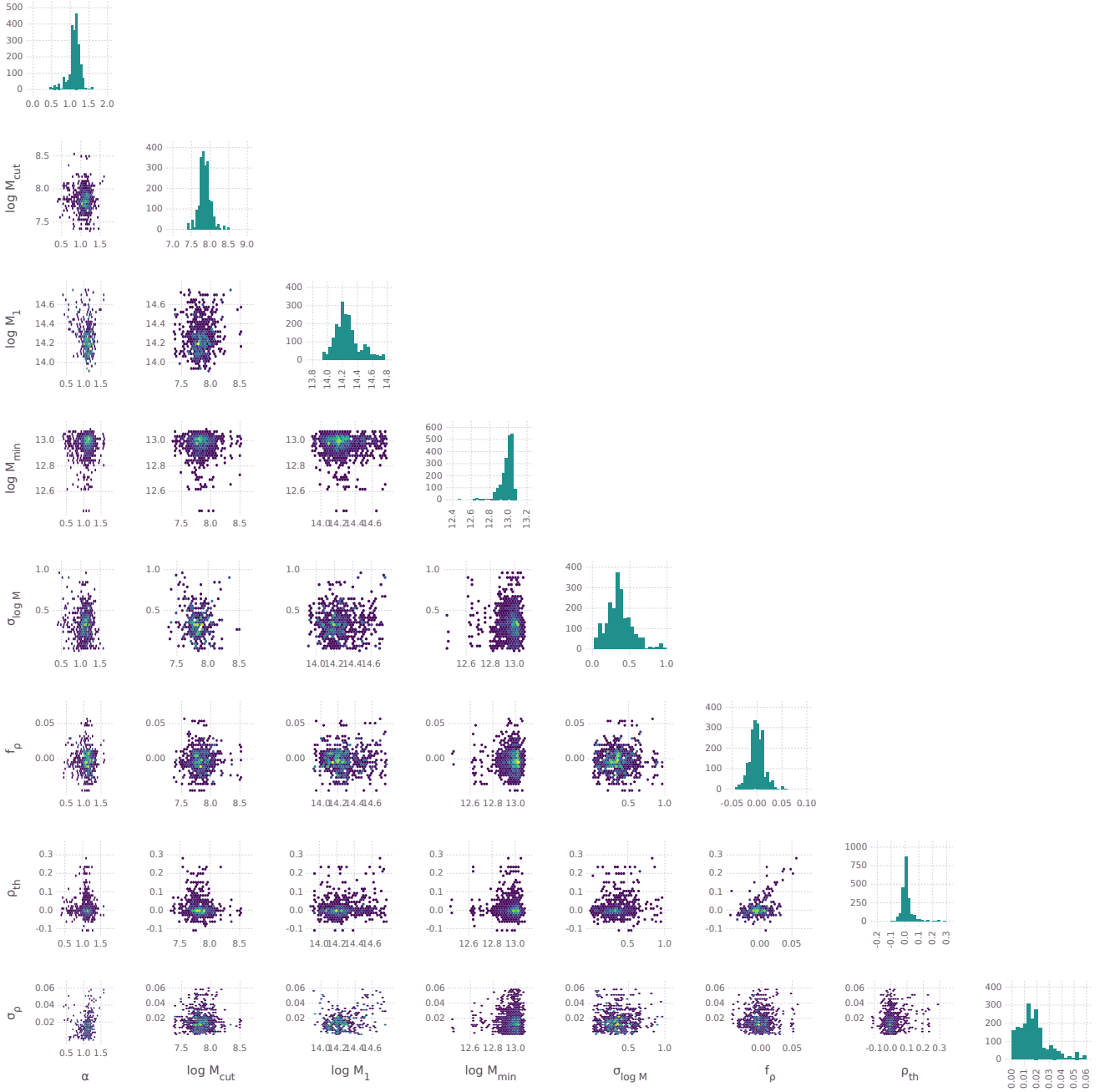


Figure 6. Here we show the posterior samples for the model described in Section 3.3 when fitting to w_p and P_0 from the CMASS northern sample including assembly bias parameters.

detection of assembly bias for the brightest samples that they examine: $M_r - 5 \log h < -21$ and -22 , respectively. The CMASS sample is not immediately comparable to a volume-limited, complete SDSS sample, but the number density of the CMASS sample is roughly consistent with the number density of the $M_r - 5 \log h < -21.5$ sample, given some grounding of the halo mass scales involved in each sample.

Additionally, the CMASS sample, as well as the brighter SDSS samples, are comprised almost exclusively of red-and-dead, passive galaxies. Many studies of color-dependent clus-

tering have shown that the quenching process cannot correlate with halo formation history (Tinker et al. 2008b, 2017, 2018; Zu & Mandelbaum 2018; Sin et al. 2017). Additionally, the small observed scatter between halo mass and stellar mass for massive galaxies is most easily explained by a quenching process that depends exclusively on the galaxy stellar mass (Tinker (2017)). Thus, galaxy quenching may erase any correlation between galaxy mass and halo formation history that may exist for star-forming galaxies which

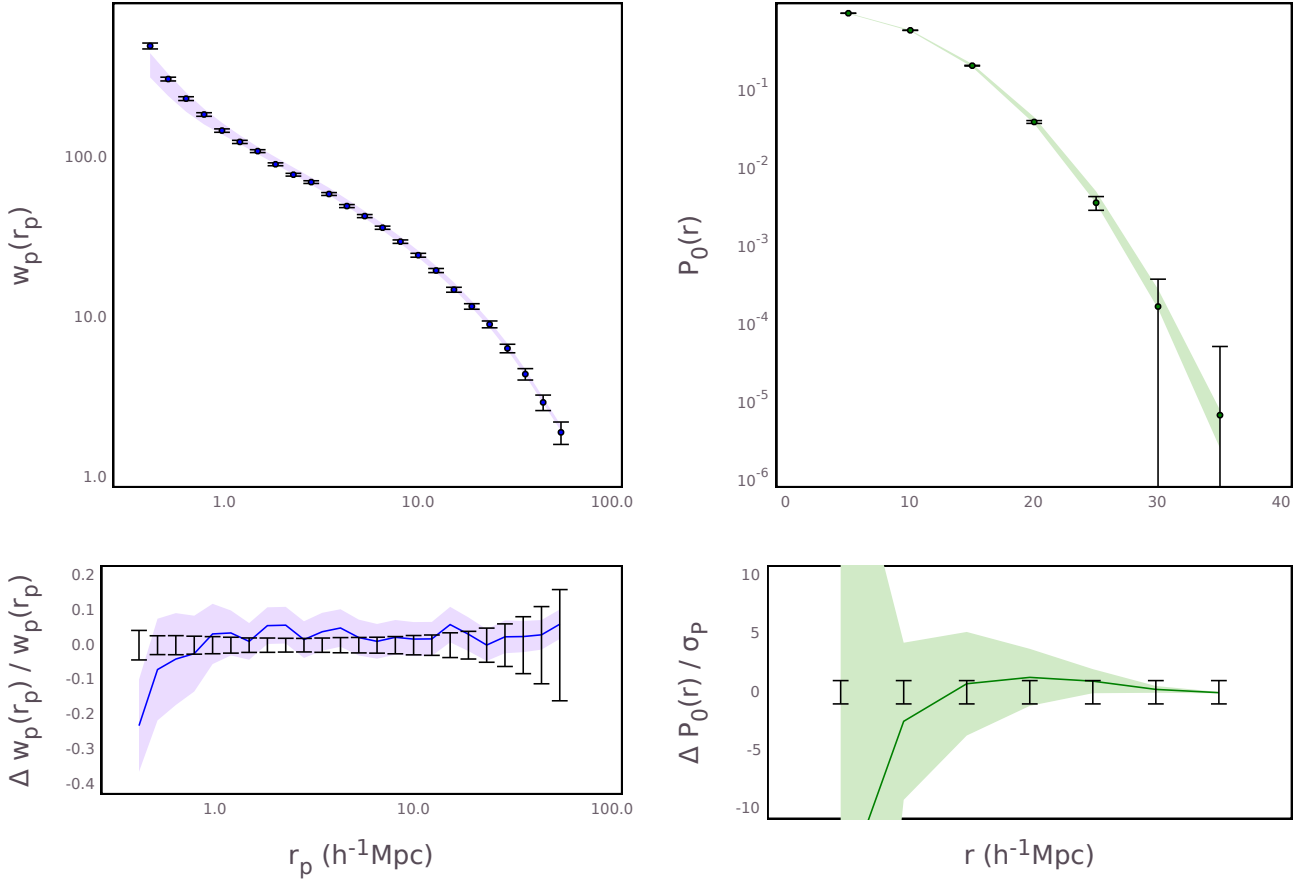


Figure 7. This figure is analogous to what is shown in Figure 5, however, in this case, the mock results are derived from posterior predicted galaxy samples from a HOD model incorporating density dependence, using parameters sampled from the posteriors shown in Figure 6

gave rise to the positive detections of galaxy assembly bias for lower-luminosity SDSS galaxies.

Thus, the luminous red galaxy class of targets may be the best opportunity to obtain cosmological constraints from non-linear galaxy clustering.

REFERENCES

- Anderson L., et al., 2014, *MNRAS*, **441**, 24
 Behroozi P. S., Wechsler R. H., Wu H.-Y., 2013, *ApJ*, **762**, 109
 Berlind A. A., Weinberg D. H., 2002, *ApJ*, **575**, 587
 Betancort-Rijo J., Patiri S. G., Prada F., Romano A. E., 2009, *MNRAS*, **400**, 1835
 Beygu B., Peletier R. F., van der Hulst J. M., Jarrett T. H., Kreckel K., van de Weygaert R., van Gorkom J. H., Aragon-Calvo M. A., 2017, *MNRAS*, **464**, 666
 Clampitt J., Jain B., Sánchez C., 2016, *MNRAS*, **456**, 4425
 Cooray A., Sheth R., 2002, *Phys. Rep.*, **372**, 1
 Coupon J., et al., 2015, *MNRAS*, **449**, 1352
 Croton D. J., Farrar G. R., 2008, *MNRAS*, **386**, 2285
 DESI Collaboration et al., 2016, preprint, ([arXiv:1611.00036](https://arxiv.org/abs/1611.00036))
 Dalal N., White M., Bond J. R., Shirokov A., 2008, *ApJ*, **687**, 12
 Davis M., Peebles P. J. E., 1983, *ApJ*, **267**, 465
 Dawson K. S., et al., 2013, *AJ*, **145**, 10
 Dawson K. S., et al., 2015, *ArXiv:1508.04473*,
 Desjacques V., Jeong D., Schmidt F., 2018, *Phys. Rep.*, **733**, 1
 Dutton A. A., Macciò A. V., 2014, *MNRAS*, **441**, 3359
 Einasto J., et al., 2011, *A&A*, **534**, A128
 Eisenstein D. J., et al., 2011, *AJ*, **142**, 72
 Goh T., et al., 2019, *MNRAS*, **483**, 2101
 Goodman J., Weare J., 2010, *Communications in Applied Mathematics and Computational Science*, Vol. 5, No. 1, p. 65-80, 2010, **5**, 65
 Gregory S. A., Thompson L. A., 1978, *ApJ*, **222**, 784
 Hearin A. P., Zentner A. R., van den Bosch F. C., Campbell D., Tollerud E., 2016, *MNRAS*, **460**, 2552
 Kitaara F.-S., et al., 2016, *Phys. Rev. Lett.*, **116**, 171301
 Klypin A., Yepes G., Gottlöber S., Prada F., Heß S., 2016, *MNRAS*, **457**, 4340
 Landy S. D., Szalay A. S., 1993, *ApJ*, **412**, 64
 Lavaux G., Wandelt B. D., 2012, *ApJ*, **754**, 109
 Lehmann B. V., Mao Y.-Y., Becker M. R., Skillman S. W., Wechsler R. H., 2017, *ApJ*, **834**, 37
 Mao Q., Berlind A. A., Scherrer R. J., Neyrinck M. C., Scoccamarro R., Tinker J. L., McBride C. K., Schneider D. P., 2017, *ApJ*, **835**, 160
 McCarthy K. S., Zheng Z., Guo H., 2018, *arXiv e-prints*, p. [arXiv:1810.05183](https://arxiv.org/abs/1810.05183)
 Mo H. J., White S. D. M., 1996, *MNRAS*, **282**, 347

- Patiri S. G., Prada F., Holtzman J., Klypin A., Betancort-Rijo J., 2006, *MNRAS*, **372**, 1710
- Planck Collaboration et al., 2018, arXiv e-prints, p. [arXiv:1807.06209](#)
- Prada F., Klypin A. A., Cuesta A. J., Betancort-Rijo J. E., Primack J., 2012, *MNRAS*, **423**, 3018
- Press W. H., Schechter P., 1974, *ApJ*, **187**, 425
- Pustilnik S. A., Tepliakova A. L., Makarov D. I., 2019, *MNRAS*, **482**, 4329
- Reddick R. M., Wechsler R. H., Tinker J. L., Behroozi P. S., 2013, *ApJ*, **771**, 30
- Reid B. A., Seo H.-J., Leauthaud A., Tinker J. L., White M., 2014, *MNRAS*, **444**, 476
- Reid B., et al., 2016, *MNRAS*, **455**, 1553
- Riebe K., et al., 2013a, *Astronomische Nachrichten*, **334**, 691
- Riebe K., et al., 2013b, *Astronomische Nachrichten*, **334**, 691
- Rodríguez-Torres S. A., et al., 2016, *MNRAS*, **460**, 1173
- Ross A. J., et al., 2017, *MNRAS*, **464**, 1168
- Saito S., et al., 2016, *MNRAS*, **460**, 1457
- Scoccimarro R., Sheth R. K., Hui L., Jain B., 2001, *ApJ*, **546**, 20
- Sheth R. K., Tormen G., 2004, *MNRAS*, **350**, 1385
- Sin L. P. T., Lilly S. J., Henriques B. M. B., 2017, *MNRAS*, **471**, 1192
- Sinha M., Garrison L., 2017, Corrfunc: Blazing fast correlation functions on the CPU, Astrophysics Source Code Library (ascl:1703.003)
- Springel V., 2005, *MNRAS*, **364**, 1105
- Tavasoli S., Rahmani H., Khosroshahi H. G., Vasei K., Lehnert M. D., 2015, *ApJ*, **803**, L13
- Tinker J. L., 2017, *MNRAS*, **467**, 3533
- Tinker J. L., Conroy C., 2009, *ApJ*, **691**, 633
- Tinker J. L., Weinberg D. H., Warren M. S., 2006, *ApJ*, **647**, 737
- Tinker J. L., Conroy C., Norberg P., Patiri S. G., Weinberg D. H., Warren M. S., 2008a, *ApJ*, **686**, 53
- Tinker J. L., Conroy C., Norberg P., Patiri S. G., Weinberg D. H., Warren M. S., 2008b, *ApJ*, **686**, 53
- Tinker J. L., et al., 2012, *ApJ*, **745**, 16
- Tinker J. L., Wetzel A. R., Conroy C., Mao Y.-Y., 2017, *MNRAS*, **472**, 2504
- Tinker J. L., Hahn C., Mao Y.-Y., Wetzel A. R., Conroy C., 2018, *MNRAS*, **477**, 935
- Wechsler R. H., Tinker J. L., 2018, *ARA&A*, **56**, 435
- Wechsler R. H., Zentner A. R., Bullock J. S., Kravtsov A. V., Allgood B., 2006, *ApJ*, **652**, 71
- Weinberg D. H., Mortonson M. J., Eisenstein D. J., Hirata C., Riess A. G., Rozo E., 2013, *Phys. Rep.*, **530**, 87
- White M., et al., 2011, *ApJ*, **728**, 126
- White M., Tinker J. L., McBride C. K., 2014, *MNRAS*, **437**, 2594
- York D. G., et al., 2000, *AJ*, **120**, 1579
- Zehavi I., et al., 2011, *ApJ*, **736**, 59
- Zentner A. R., 2007, *International Journal of Modern Physics D*, **16**, 763
- Zentner A. R., Hearin A. P., van den Bosch F. C., 2014, *MNRAS*, **443**, 3044
- Zentner A. R., Hearin A., van den Bosch F. C., Lange J. U., Villarreal A., 2016, *MNRAS*, submitted, ArXiv:1606.07817,
- Zhai Z., et al., 2018, *ApJ*, submitted, ArXiv:1804.05867,
- Zheng Z., Coil A. L., Zehavi I., 2007, *ApJ*, **667**, 760
- Zu Y., Mandelbaum R., 2018, *MNRAS*, **476**, 1637
- van de Weygaert R., Platen E., 2011, in *International Journal of Modern Physics Conference Series*. pp 41–66 ([arXiv:0912.2997](#)), doi:10.1142/S2010194511000092

This paper has been typeset from a \LaTeX file prepared by the author.